Inorganic Chemistry

pubs.acs.org/IC

Article

[Au^{I}(CN)$_2$]-Armed [Fe$^{III}_2$Fe$^{II}_2$] Square Complex Showing Unusual Spin-Crossover Behavior Due to a Symmetry-Breaking Phase Transition

Maolin You, Dong Shao, Yi-Fei Deng,* Jiong Yang, Nian-Tao Yao, Yin-Shan Meng, Liviu Ungur, and Yuan-Zhu Zhang*

Cite This: *Inorg. Chem.* 2022, 61, 5855−5860

Read Online

ACCESS | Metrics & More | Article Recommendations | Supporting Information

ABSTRACT: The incorporation of two different cyanide building blocks of [(Tp^{R})Fe^{III}(CN)$_3$]$^-$ and [Au^{I}(CN)$_2$]$^-$ into one molecule afforded a novel hexanuclear [Fe$^{III}_2$Fe$^{II}_2$Au$^{I}_2$] complex (**1·2Et$_2$O**), in which the cyanide-bridged [Fe$^{III}_2$Fe$^{II}_2$] square was further grafted by two [Au^{I}(CN)$_2$]$^-$ fragments as long arms in *syn* orientations. Complex **1·2Et$_2$O** undergoes a gradual spin crossover (SCO) ffrom low-spin (LS) to high-spin (HS) state for the Fe(II) centers upon desolvation. Remarkably, its desolvated phase (**1**) exhibits a reversible but atypical two-step (sharp−gradual) SCO behavior with considerable hysteresis (21 K). Variable-temperature single-crystal X-ray structural studies reveal that the hysteretic spin transition takes place synchronously with the concerted displacive motions of the molecules, representing another rare example including multistep and hysteretic spin transitions due to the synergetic SCO and structural phase transition.

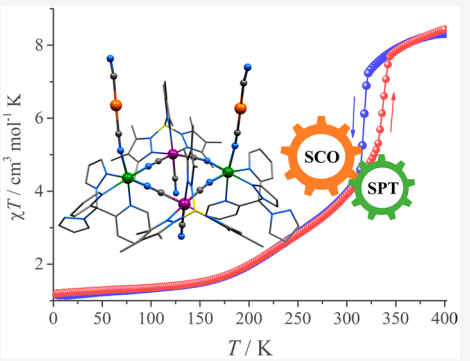

INTRODUCTION

The mixed-valence cyanometallate complexes that feature either metal-to-metal charge transfer (MMCT) or spin crossover (SCO) in response to temperature, light, pressure, and other external stimuli have attracted a considerable amount of attention since Hashimoto et al. reported the first magnetically photoswitchable Prussian blue analogue (PBA), $K_{0.2}Co_{1.4}[Fe(CN)_6]\cdot 6.9H_2O$, in 1996.[1−4] These three-dimensional (3D) coordination networks showed tunable magnetic bistabilities,[5] which however strongly depend on the reagent stoichiometry, synthetic procedures, and sample history due to the rich lattice defects. The related studies demonstrated an average [N$_5$O] coordination sphere may activate the MMCT for this system.[6] A key underpinning of the research on this topic is a thorough understanding of the molecular design toward specific structural architectures and/or desired functionalities.[7] In this frame, the building-block approach is by no means a good idea for achieving this goal. Dunbar and co-workers subsequently moved the research forward with a series of cyano-bridged trigonal bipyramidal {Fe$_2$Co$_3$} complexes by using bidentate ligands.[8]

Notably, the application of poly(pyrazolyl)borate tricyanoiron(III) {[(Tp^{R})Fe^{III}(CN)$_3$]$^-$} building blocks with different metal ions and capping ligands has led to a wide diversity of structural motifs such as squares,[9] cubes,[10] and chains,[11] some of which exhibit single-molecule magnet (SMM), single-chain magnet (SCM), SCO, or MMCT properties. For example, Li et al. reported the first molecular [Fe$_4$Co$_4$] cube[12] that mimics both the structural motif and MMCT properties of 3D PB analogues with the existence of the tridentate capping ligand 2,2,2-tris(pyrazolyl)ethanol; quite a considerable number of molecular squares showing either MMCT or SCO properties were well constructed when using tetradentate or double bidentate chelated ligands.[13]

The great progress of these discrete magnetically switchable molecules notwithstanding, most of them exhibit no or only a small thermal hysteresis due to the lack of strong cooperativity, which strongly determines the nature (the speed and hysteresis) of the spin transition.[14,15] To address this question, one of the most successful synthetic routes is linking the Fe(II) centers by the square-planar [M^{II}(CN)$_4$]$^{2-}$ (M = Ni, Pt, or Pd) or linear [M^{I}(CN)$_2$]$^-$ (M = Au or Ag) cyanometalate, which has led to a large family of Hofmann-type SCO coordination polymers.[16] Generally, these coordination compounds often exhibit sharp and hysteretic SCO behaviors due to the strong cooperativity mediated through the high-dimensional elastic interaction.[17] In these respects, these cyanometalates are naturally great metalloligands for the design of high-performance SCO behavior.

Because of the considerations described above and our continuous interest in cyanometallate complexes based on [(Tp^{R})Fe^{III}(CN)$_3$]$^-$ units, we presumed that the SCO-active square-like PBA motifs may be linked into a polymeric crystal

Received: January 19, 2022
Published: April 4, 2022

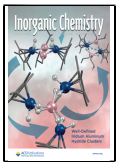

https://doi.org/10.1021/acs.inorgchem.2c00192
Inorg. Chem. 2022, 61, 5855−5860

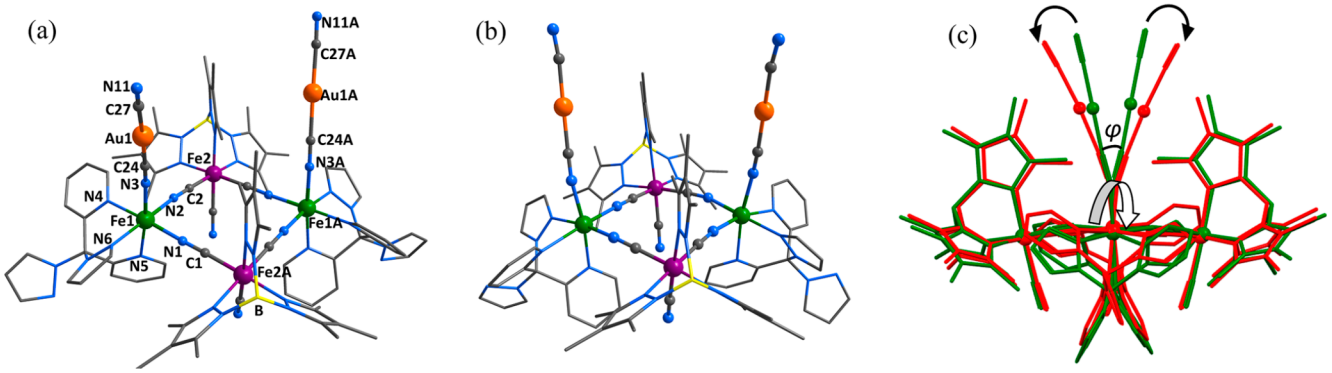

Figure 1. Molecular structures of (a) **1·2Et$_2$O** and (b) **1** at 350 K and (c) their minimized overlay. The hydrogen atoms and lattice solvent molecules have been omitted for the sake of clarity.

lattice by means of linear $[Au(CN)_2]^-$ bridges. Here, we report a neutral hexanuclear $[Fe^{III}_2Fe^{II}_2Au^{I}_2]$ (**1·2Et$_2$O**) complex, in which a cyanide-bridged $[Fe^{III}_2Fe^{II}_2]$ molecular square was further grafted with two linear $[Au(CN)_2]^-$ metalloligands in the *syn* orientational mode. Both magnetic and structural studies revealed that **1·2Et$_2$O** underwent gradual SCO upon desolvation, accompanied by an irriversible phase transition at high temperatures. Interestingly, its desolvated phase (**1**) exhibits a complete two-step spin transition, including a gradual, nonhysteretic SCO and an abrupt, hysteretic SCO (~20 K) near room temperature. Detailed structural analyses revealed that the hysteretic transition in **1** is due to the synergetic SCO and symmetry-breaking structural phase transition.

RESULTS AND DISCUSSION

Synthesis and Crystallographic Studies. Slow diffusion of diethyl either (Et_2O) into a mixed acetonitrile and methanol solution containing $[(Tp^{*Me})Fe^{III}(CN)_3]^-$, $Fe(OTf)_2$, di(1*H*-pyrazol-1-yl)di(pyridin-2-yl)methane (L), and $KAu(CN)_2$ in a 1:1:1:1 molar ratio afforded dark red crystals of $[(Tp^{*Me})Fe^{III}(CN)_3Fe^{II}(L)Au^{I}(CN)_2]_2\cdot 2Et_2O$ [**1·2Et$_2$O**, where Tp^{*Me} = tris(3,4,5-trimethylpyrazole)borate (details in the experimental section of the Supporting Information)]. Thermogravimetric analysis (TGA) revealed that the lattice solvent molecules were essentially stable below 90 °C, after which a one-step desolvation took place with a weight loss of 6.35% [calcd 6.42% (Figure S1)]. The following plateau up to 210 °C suggested the considerable thermal stability of the desolvated phase, which was further characterized as complex **1** by both single-crystal and powder X-ray diffraction. In fact, the single crystals of **1** could be obtained by heating the fresh crystals of **1·2Et$_2$O** at 400 K for 10 min, and the bulk sample of **1** was purely prepared by heating **1·2Et$_2$O** under N_2 at 125 °C for 30 min. The purity of both **1·2Et$_2$O** and **1** was confirmed by powder X-ray diffraction measurements, which match well with their single-crystal simulations (Figures S2 and S3).

Single-crystal X-ray diffraction (SCXRD) analysis revealed that **1·2Et$_2$O** crystallized in the monoclinic *C*2/*c* space group (Table S1). Due to the 2-fold (C_2) symmetry, the asymmetric unit contains half of the molecular core as well as lattice solvent molecules. As shown in Figure 1a, the cyanide-bridged $[(Tp^{*Me})Fe^{III}(CN)_3]^-$ and $[(L)Fe^{II}]$ units reside in alternate corners of a molecular square, with two $[Au^{I}(CN)_2]^-$ units being grafted on the Fe(II) centers in *syn* orientations via cyanide groups. Enclosed within the square, the Fe−C≡N−Fe cyano linkages are nearly linear with Fe−C≡N and C≡N−Fe bond angles in the range of 177.8(5)−178.8(5)° and 174.4(1)−177.1(2)°, respectively. Each Fe1 is chelated by two pyrazole N atoms and one pyridine N atom from ligand L, with three cyanides completing the Fe−N6 octahedral coordination environment. The Fe1−N bond distances at 100 K are in the range of 1.923(5)−2.005(5) Å, with the average value being 1.954(5) Å at 100 K, typical for an Fe(II) ion in the low-spin (LS) state (Table S3).[14] Upon heating, the average Fe1−N bond distance increases slightly to 1.974(6) Å at 300 K, and clearly to 2.031(5) Å at 350 K, suggesting a mixture containing both high-spin (HS) and LS Fe(II) species. It should be mentioned that higher-temperature crystal data for **1·2Et$_2$O** are not available due to the loss of lattice solvent molecules.

The SCXRD analysis for **1** at 350 K indicated that desolvated complex **1** also crystallized in the monoclinic *C*2/*c* space group (Figure 1b and Table S2). The average Fe1−N bond distance is 2.148(2) Å, close to those (~2.18 Å) for the reported HS Fe^{II} complexes (Table S4).[18] Interestingly, the minimized overlay of the molecular structures for **1·2Et$_2$O** and **1** at 350 K revealed a clear conformational change involving a scissor-like structural rearrangement of the $[Au(CN)_2]^-$ metalloligands and a rotation in the aromatic rings of L ligands (Figure 1c). Specifically, the twist angle of 25.1° between N3−C24−Au1 and Au1A−N3A−C24A for **1** is much smaller than that (42.1°) for **1·2Et$_2$O**, and the L and Tp^{*Me} ligands around Fe1 and Fe2 in **1** rotate by 14.2° and 7.8°, respectively, referenced to those in **1·2Et$_2$O**, giving a root-mean-square deviation (RMSD) of 0.8915. Combined with packing structures as well as Hirshfeld surface analyses, different weak intercluster interactions are evidenced, such as the C−H···N [2.590(1) and 2.659(6) Å] interaction (17.9%) in **1·2Et$_2$O** and the C−H···N [2.629(2), 2.697(2), and 2.858(1) Å] (19.7%), C−H···π [2.642(4) and 2.742(2) Å], and $\pi\cdots\pi$ [3.760(1) Å] interactions in **1** (Figures S4−S7).

FT-IR Studies. To possibly exclude the MMCT event for such a system and track the dynamic variations of valences and spin states of the iron ions, variable-temperature infrared spectra (VT-IR) were recorded (Figures S8 and S9). At 300 K, **1·2Et$_2$O** exhibited a ν_{BH} absorption peak at 2536 cm^{-1} and a group of peaks in the range of 2100−2200 cm^{-1} for the cyanide stretches. The shoulder peaks at 2141 and 2124 cm^{-1} are assigned to the bridging and terminal cyanides, respectively, of the $[(Tp^{*Me})Fe^{III}(CN)_3]^-$ species, according to the related literature,[9b,14d] while the sharp peak at 2147

https://doi.org/10.1021/acs.inorgchem.2c00192
Inorg. Chem. 2022, 61, 5855−5860

cm^{-1} and the shoulder one at 2170 cm^{-1} may be assigned to the coordinated and uncoordinated ν_{CN} stretches, respectively, of the $[Au^{I}(CN)_2]^-$ units.[19] Upon heating, the peaks at 2141 and 2124 cm^{-1} slightly shifted to higher wavenumbers with increased intensity, likely due to the spin transition on the Fe^{II} ions. During the subsequent cooling measurements, the change in the spectra of **1** was similar to that of **1·2Et$_2$O**, suggesting that the SCO property is preserved for **1**. The absence of ν_{CN} stretches below 2100 cm^{-1} for both **1·2Et$_2$O** and **1** in the whole recorded temperature range clearly excludes the appearance of $[(Tp^{*Me})Fe^{II}(CN)_3]^{2-}$ anions, thus suggesting that no electron transfer occurred between $[Fe^{III}-CN-Fe^{II}]$ linkages.

Magnetic Studies. Variable-temperature magnetic susceptibility data for the fresh sample of **1·2Et$_2$O** (per $[Fe^{III}_2Fe^{II}_2Au^{I}_2]$ unit) were measured under an applied direct current (dc) field of 1 kOe with a sweep rate of 2 K/min (Figure 2). Below 200 K, the χT product nearly remains

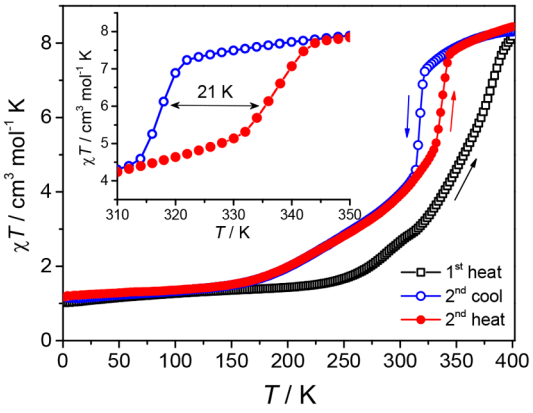

Figure 2. Variable-temperature magnetic susceptibility data with a sweeping rate of 2 K/min for **1·2Et$_2$O** (black data points) and *in situ*-generated **1** (blue, cooling; red, heating). The inset is a close-up between 310 and 350 K.

constant at 1.23 cm^3 mol^{-1} K, corresponding to two LS Fe^{III} (S = 1/2) ions with a considerable orbital contribution.[9] Upon heating, the χT product increases gradually to 8.40 cm^3 mol^{-1} K at 400 K, consistent with two LS Fe^{III} and two HS Fe^{II} (S = 2) ions and indicating a complete LS → HS spin transition accompanied by desolvation. The desolvated analogue (**1**) was obtained *in situ* by continuously heating the sample of **1·2Et$_2$O** at 400 K for 10 min in the magnetometer. With a decrease in temperature, the χT values of **1** slowly decrease to 320 K and then drop abruptly to ∼4.30 cm^3 mol^{-1} K^{-1} at 310 K, followed by a gradual decrease until stabilizing around 1.38 cm^3 mol^{-1} K below 120 K. With an increase in temperature, the variation of χT follows the same trail as seen in the cooling mode below 310 K while exhibiting a clear thermal hysteresis (∼21 K wide), which is well reproduced over the following cycles of measurements (Figure S10). It should be mentioned that the continuous increase in the χT values above 350 K indicates the gradual ongoing uncompleted SCO transition. This observation also explains why the average Fe1−N bond distance [2.148(2) Å] for **1** at 350 K is shorter than the typical HS Fe^{II}−N distance (∼2.18 Å).

To clarify the unusual magnetic behavior of **1**, variable-temperature SCXRD experiments were conducted. During the cooling from 350 to 300 K, a symmetry-breaking structural phase transition was observed, where the crystalline *a* and *b* axes doubled, yielding a quadrupling of the unit cell volume. Consequently, the asymmetric unit at 300 K comprises two squares, including a square of C and a half-square of B and D (Figure 3). These changes in the cell parameters contributed to a significant variation in the conformational arrangements. Specifically, the dihedral angels of squares B−D decrease to 16.2°, 19.4°, and 17.6°, respectively; clear rotations of ligands L and Tp^{*Me} were also observed, when being overlaid with those at 350 K (Figure S11). Additionally, the average Fe^{II}−N bond distances of squares B−D are 2.135(9), 1.982(8), and 1.959(9) Å, respectively, suggesting an intermediate phase with the presence of 1/4 HS and 3/4 LS Fe^{II} species. In terms of the driving force for the symmetry-breaking phase transition in **1**, the molecular volume change accompanying the gradual SCO process may be an important reason to trigger such a phenomenon once the threshold spin-conversion ratio is achieved.[20] Moreover, the grafted $[Au^{I}(CN)_2]^-$ fragments serving as flexible arms may also help contribute to the abrupt phase transition in **1**, as commonly observed in soft SCO compounds.[21] It is worth mentioning that no significant change in the supramolecular interactions was observed on the basis of the Hirshfeld surface analyses for **1** at 350 K versus 300 K (Figures S6, S7, S12, and S13). At 300 K, the dominant supramolecular interactions (C−H···N, C−H···π, and π···π interactions) are comparable with those at 350 K, with a slight

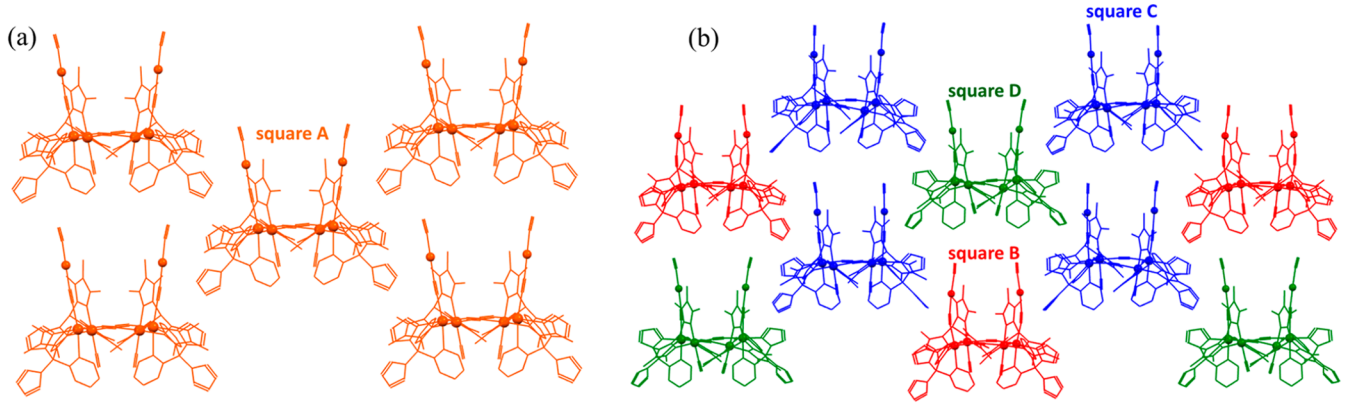

Figure 3. Packing structures of **1** at 350 K (a, containing only one type of square, A) and 300 K (b, containing three different types of squares, B−D), indicating the symmetry-breaking structural phase transition.

https://doi.org/10.1021/acs.inorgchem.2c00192
Inorg. Chem. 2022, 61, 5855−5860

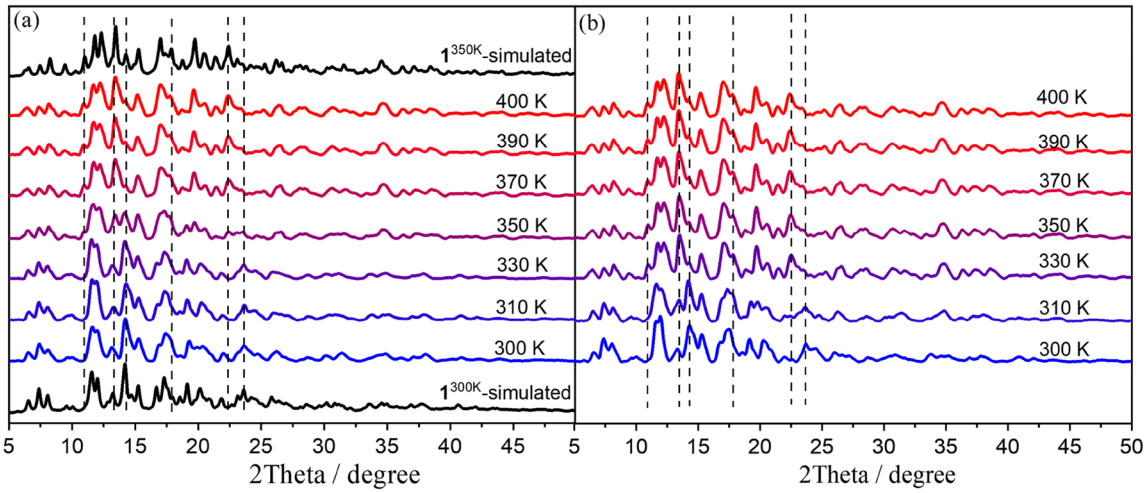

Figure 4. Variable-temperature powder X-ray diffraction for **1** in the (a) heating and (b) cooling modes. The simulated patterns for **1** are calculated on the basis of the single-crystal data.

decrease in the percentage contribution for the C−H···N contacts (18.3%). Such behavior is reminiscent of a recent work in which the broad hysteretic spin transition of a Fe^{II} compound arises from an interplay between the SCO and symmetry-breaking SPT rather than from a strong cooperativity mediated by the supramolecular interaction.[20] When the temperature is further decreased from 300 to 100 K, the structures of the intermediate phase were found to remain (Figure S14), while the average Fe^{II}−N bond distances of squares B−D decreased to 1.964(6), 1.950(7), and 1.953(6) Å, respectively, typical for the pure LS Fe^{II} ions. As such, these results clearly corroborate that the first-step abrupt transition between 350 and 300 K is attributed to the synergetic SCO and symmetry-breaking structural phase transition;[22] the second-step gradual transition is caused by the SCO event.

PXRD and DSC Studies. The validity of related structural phase transitions obtained from SC-XRD studies for its respective bulk samples was further investigated through variable-temperature powder X-ray diffraction (Figure 4) and DSC experiments. For desolvated sample **1**, during the heating cycle, the PXRD patterns remained almost unchanged from 300 to 330 K. When the temperature is further increased to 350 K, three new PXRD peaks at ∼10.9°, ∼17.9°, and ∼22.5° appeared, the intensity of the peaks at 14.2° and 23.6° increased, and the intensity of the peak at 13.4° decreased (Figure 4a). Further increasing the temperature does not reveal any significant changes. During the subsequent cooling cycle (Figure 4b), the PXRD patterns revealed the reverse changes from 330 to 310 K compared with those observed at 330−350 K in the heating mode. These results suggested a reversible phase transition proceeded during the heating and cooling cycles between 310 and 350 K. Moreover, the phase transitions were also supported by the differential scanning calorimetry (DSC) measurements. During heating for **1·2Et$_2$O**, a broad endothermic peak (ΔH = 35.8 kJ mol^{-1}, and ΔS = 91.8 J mol^{-1} K^{-1}) was observed at 390 K, suggesting a phase transition during the desolvation process (Figure S15). For **1**, a pair of sharp endothermic and exothermic peaks at 310 and 320 K are found with a ΔH of 9.45 kJ mol^{-1} and a ΔS of 30.5 J mol^{-1} K^{-1} and a ΔH of 8.58 kJ mol^{-1} and a ΔS of 26.8 J mol^{-1} K^{-1}, respectively (2 K/min), confirming the presence of a structural phase transition that is consistent with the SCXRD and magnetic studies (Figure S16). Additionally, to investigate whether the electronic polarizability can be tuned through structural phase transitions and electron rearrangements, the dielectric constant of **1** was measured over the temperature and frequency ranges of 100−400 K and 0.5−100 kHz, respectively (Figure S17). As a result, two broad dielectric anomalies were observed at ∼320 and ∼270 K with moderate frequency-dependent behavior. Such a phenomenon is reasonably correlated with the two-step spin transitions that cause the changes in the local polarizability that contribute to the dielectric constant.[11b,23]

CONCLUSIONS

In summary, we present a detailed structural and magnetic study of a hexanuclear $[Fe^{III}_2Fe^{II}_2Au^{I}_2]$ complex in the solvated (**1·2Et$_2$O**) and desolvated (**1**) phases. **1·2Et$_2$O** exhibits a gradual and complete SCO upon desolvation, accompanying a phase transition caused by the scissor-like structural rearrangement of the $[Au(CN)_2]^-$ metalloligands and the rotation in the aromatic rings of chelating ligand L. The desolvated phase **1**, however, undergoes a two-step and hysteretic spin transition. Variable-temperature SCXRD and PXRD studies revealed that the first-step abrupt and hysteretic magnetic transition between 350 and 300 K originated from a synergetic effect between SCO and SPT via concerted molecular displacive motions; the second-step magnetic transition was solely caused by the gradual SCO event. As such, we present a rare example of achieving a multistep and hysteretic spin transition through the synergetic SCO and symmetry-breaking structural phase transition. Molecular engineering on such square motifs with more attachments to promote the cooperativity or synergy of the system is in progress.

ASSOCIATED CONTENT

Supporting Information

The Supporting Information is available free of charge at https://pubs.acs.org/doi/10.1021/acs.inorgchem.2c00192.

Procedures, X-ray crystallographic data, crystal structures, thermogravimetric analysis data, DSC curves, and magnetic data (PDF)

https://doi.org/10.1021/acs.inorgchem.2c00192
Inorg. Chem. 2022, 61, 5855−5860

Accession Codes

CCDC 2086214−2086219 contain the supplementary crystallographic data for this paper. These data can be obtained free of charge via www.ccdc.cam.ac.uk/data_request/cif, or by emailing data_request@ccdc.cam.ac.uk, or by contacting The Cambridge Crystallographic Data Centre, 12 Union Road, Cambridge CB2 1EZ, UK; fax: +44 1223 336033.

AUTHOR INFORMATION

Corresponding Authors

Yi-Fei Deng − *Department of Chemistry, Southern University of Science and Technology (SUSTech), Shenzhen 518055, China*; Email: dengyf@sustech.edu.cn

Yuan-Zhu Zhang − *Department of Chemistry, Southern University of Science and Technology (SUSTech), Shenzhen 518055, China*; orcid.org/0000-0002-1676-2427; Email: zhangyz@sustech.edu.cn

Authors

Maolin You − *Department of Chemistry, Southern University of Science and Technology (SUSTech), Shenzhen 518055, China; Department of Chemistry, National University of Singapore, Singapore 117543*

Dong Shao − *Department of Chemistry, Southern University of Science and Technology (SUSTech), Shenzhen 518055, China*; orcid.org/0000-0002-3253-2680

Jiong Yang − *Department of Chemistry, Southern University of Science and Technology (SUSTech), Shenzhen 518055, China*

Nian-Tao Yao − *State Key Laboratory of Fine Chemicals, Dalian University of Technology, Dalian 116024, China*

Yin-Shan Meng − *State Key Laboratory of Fine Chemicals, Dalian University of Technology, Dalian 116024, China*; orcid.org/0000-0001-9963-4596

Liviu Ungur − *Department of Chemistry, National University of Singapore, Singapore 117543*; orcid.org/0000-0001-5015-4225

Complete contact information is available at: https://pubs.acs.org/10.1021/acs.inorgchem.2c00192

Notes

The authors declare no competing financial interest.

ACKNOWLEDGMENTS

This work was supported by the Stable Support Plan Program of Shenzhen Natural Science Fund (20200925151834005) and the National Natural Science Foundation of China (21901108 and 22173043).

REFERENCES

(1) Sato, O.; Iyoda, T.; Fujishima, A.; Hashimoto, K. Photoinduced Magnetization of a Cobalt-Iron Cyanide. *Science* **1996**, *272*, 704−705.

(2) Kahn, O.; Martinez, C. J. Spin-Transition Polymers: From Molecular Materials Toward Memory Devices. *Science* **1998**, *279*, 44−48.

(3) Sato, O.; Tao, J.; Zhang, Y.-Z. Control of Magnetic Properties through External Stimuli. *Angew. Chem., Int. Ed.* **2007**, *46*, 2152−2187.

(4) Ohkoshi, S.-I.; Tokoro, H. Photomagnetism in Cyano-Bridged Bimetal Assemblies. *Acc. Chem. Res.* **2012**, *45*, 1749−1758.

(5) Aguilà, D.; Prado, Y.; Koumousi, E. S.; Mathoniére, C.; Clérac, R. Switchable Fe/Co Prussian Blue Networks and Molecular Analogues. *Chem. Soc. Rev.* **2016**, *45*, 203−224.

(6) (a) Cafun, J.-D.; Champion, G.; Arrio, M.-A.; Cartier dit Moulin, C.; Bleuzen, A. Photomagnetic CoFe Prussian Blue Analogues: Role of the Cyanide Ions as Active Electron Transfer Bridges Modulated by Cyanide−Alkali Metal Ion Interactions. *J. Am. Chem. Soc.* **2010**, *132*, 11552−11559. (b) Cammarata, M.; Zerdane, S.; Balducci, L.; Azzolina, G.; Mazerat, S.; Exertier, C.; Trabuco, M.; Levantino, M.; Alonso-Mori, R.; Glownia, J. M.; Song, S.; Catala, L.; Mallah, T.; Matar, S. F.; Collet, E. Charge transfer driven by ultrafast spin transition in a CoFe Prussian blue analogue. *Nat. Chem.* **2021**, *13*, 10−14. (c) Bordage, A.; Moulin, R.; Fonda, E.; Fornasieri, G.; Rivière, E.; Bleuzen, A. Evidence of the Core−Shell Structure of (Photo)-magnetic CoFe Prussian Blue Analogue Nanoparticles and Peculiar Behavior of the Surface Species. *J. Am. Chem. Soc.* **2018**, *140*, 10332−10343. (d) Jafri, S. F.; Koumousi, E. S.; Arrio, M.-A.; Juhin, A.; Mitcov, D.; Rouzières, M.; Dechambenoit, P.; Li, D.; Otero, E.; Wilhelm, F.; Rogalev, A.; Joly, L. K.; Kappler, J.-P.; Cartier dit Moulin, C.; Mathonière, C.; Clérac, R.; Sainctavit, P. Atomic Scale Evidence of the Switching Mechanism in a Photomagnetic CoFe Dinuclear Prussian Blue Aalogue. *J. Am. Chem. Soc.* **2019**, *141*, 3470−3479.

(7) (a) Sato, O. Dynamic Molecular Crystals with Switchable Physical Properties. *Nat. Chem.* **2016**, *8*, 644−656. (b) Meng, Y.-S.; Sato, O.; Liu, T. Manipulating Metal-to-Metal Charge Transfer for Materials with Switchable Functionality. *Angew. Chem., Int. Ed.* **2018**, *57*, 12216−12226. (c) Huang, W.; Ma, X.; Sato, O.; Wu, D. Controlling dynamicmagnetic properties of coordination clusters via switchable electronic configuration. *Chem. Soc. Rev.* **2021**, *50*, 6832−6870.

(8) (a) Berlinguette, C. P.; Dragulescu-Andrasi, A.; Sieber, A.; Galán-Mascarós, J. R.; Güdel, H.-U.; Achim, C.; Dunbar, K. R. A Charge-Transfer-Induced Spin Transition in the Discrete Cyanide-Bridged Complex $\{[Co(tmphen)_2]_3[Fe(CN)_6]_2\}$. *J. Am. Chem. Soc.* **2004**, *126*, 6222−6223. (b) Hilfiger, M. G.; Chen, M.; Brinzari, T. V.; Nocera, T. M.; Shatruk, M.; Petasis, D. T.; Musfeldt, J. L.; Achim, C.; Dunbar, K. R. An Unprecedented Charge Transfer Induced Spin Transition in an Fe−Os Cluster. *Angew. Chem., Int. Ed.* **2010**, *49*, 1410−1413. (c) Avendano, C.; Hilfiger, M. G.; Prosvirin, A.; Sanders, C.; Stepien, D.; Dunbar, K. R. Temperature and Light Induced Bistability in a $Co_3[Os(CN)_6]_2$ $6H_2O$ Prussian Blue Analog. *J. Am. Chem. Soc.* **2010**, *132*, 13123−13125. (d) Dunbar, K. R.; Achim, C.; Shatruk, M. Charge Transfer-Induced Spin-Transitions in Cyanometallate Materials. In *Spin-Crossover Materials: Properties and Applications*; John Wiley & Sons: Hoboken, New Jersey, **2013**.

(9) (a) Zhang, Y.-Z.; Li, D.; Clérac, R.; Kalisz, M.; Mathonière, C.; Holmes, S. M. Reversible Thermally and Photoinduced Electron Transfer in a Cyano-Bridged $\{Fe_2Co_2\}$ Square Complex. *Angew. Chem., Int. Ed.* **2010**, *49*, 3752−3756. (b) Nihei, M.; Sekine, Y.; Suganami, N.; Nakazawa, K.; Nakao, A.; Nakao, H.; Murakami, Y.; Oshio, H. Controlled Intramolecular Electron Transfers in Cyanide-Bridged Molecular Squares by Chemical Modifications and External Stimuli. *J. Am. Chem. Soc.* **2011**, *133*, 3592−3600.

(10) (a) You, M.; Gan, D.-X.; Deng, Y.-F.; Shao, D.; Meng, Y.-S.; Chang, X.-Y.; Zhang, Y.-Z. Thermally Induced Reversible Metal-to-Metal Charge Transfer in Mixed-Valence $\{Fe^{III}_4Fe^{II}_4\}$ Cubes. *CCS Chem.* **2021**, 3, 2593−2600. (b) Garnier, D.; Jiménez, J.-R.; Li, Y.; von Bardeleben, J.; Journaux, Y.; Augenstein, T.; Moos, E. M. B.; Gamer, M. T.; Breher, F.; Lescouëzec, R. K ⊂ $\{[Fe^{II}(Tp)(CN)_3]_4[Co^{III}(pzTp)]_3[Co^{II}(pzTp)]\}$: a neutral soluble model complex of photomagnetic Prussian blue analogues. *Chem. Sci.* **2016**, *7*, 4825−4831.

(11) (a) Liu, T.; Zheng, H.; Kang, S.; Shiota, Y.; Hayami, S.; Mito, M.; Sato, O.; Yoshizawa, K.; Kanegawa, S.; Duan, Y.-C. A light-induced spin crossover actuated single-chain magnet. *Nat. Commun.* **2013**, *4*, 2826. (b) Zheng, H.; Meng, Y.-S.; Zhou, G.-L.; Duan, C.-Y.; Sato, O.; Hayami, S.; Luo, Y.; Liu, T. Simultaneous modulation of magnetic and dielectric transition via spin-crossover-tuned spin arrangement and charge distribution. *Angew. Chem., Int. Ed.* **2018**, *57*, 8468−8472. (c) Hu, J.-X.; Xu, Y.; Meng, Y.-S.; Zhao, L.; Hayami, S.; Sato, O.; Liu, T. A Material Showing Colossal Positive and

Negative Volumetric Thermal Expansion with Hysteretic Magnetic Transition. *Angew. Chem., Int. Ed.* **2017**, *56*, 13052−13055.
(12) Li, D.; Clérac, R.; Roubeau, O.; Harté, E.; Mathonière, C.; Le Bris, R.; Holmes, S. M. Magnetic and Optical Bistability Driven by Thermally and Photoinduced Intramolecular Electron Transfer in a Molecular Cobalt−Iron Prussian Blue Analogue. *J. Am. Chem. Soc.* **2008**, *130*, 252−258.
(13) (a) Zhang, Y.-Z.; Ferko, P.; Siretanu, D.; Ababei, R.; Rath, N. P.; Shaw, M. J.; Clérac, R.; Mathonière, C.; Holmes, S. M. Thermochromic and Photoresponsive Cyanometalate Fe/Co Squares: Toward Control of the Electron Transfer Temperature. *J. Am. Chem. Soc.* **2014**, *136*, 16854−16864. (b) Nihei, M.; Ui, M.; Yokota, M.; Han, L.; Maeda, A.; Kishida, H.; Okamoto, H.; Oshio, H. Two-step spin conversion in a cyanide-bridged ferrous square. *Angew. Chem., Int. Ed.* **2005**, *44*, 6484−6487. (c) Mondal, A.; Li, Y.; Herson, P.; Seuleiman, M.; Boillot, M. L.; Rivière, E.; Julve, M.; Rechignat, L.; Bousseksou, A.; Lescouëzec, R. Photomagnetic effect in a cyanide-bridged mixed-valence $\{Fe^{II}_2Fe^{III}_2\}$ molecular square. *Chem. Commun.* **2012**, *48*, 5653−5655. (d) Jiao, C.-Q.; Meng, Y.-S.; Yu, Y.; Jiang, W.-J.; Wen, W.; Oshio, H.; Luo, Y.; Duan, C.-Y.; Liu, T. Effect of Intermolecular Interactions on Metal-to-Metal Charge Transfer: A Combined Experimental and Theoretical Investigation. *Angew. Chem., Int. Ed.* **2019**, *58*, 17009−17015.
(14) (a) Chen, J.-T.; Zhao, X.-H.; Zhang, Y.-Z. Manipulating the spin crossover behavior in a series of $\{Fe^{III}_2Fe^{II}\}$ complexes. *Dalton Trans.* **2020**, *49*, 5949−5956. (b) Zhao, X.-H.; Shao, D.; Chen, J.-T.; Liu, M.; Li, T.; Yang, J.; Zhang, Y.-Z. Spin and Valence Isomerism in Cyanide-Bridged $\{Fe^{III}_2M^{II}\}$(M= Fe, Co) Clusters. *Dalton Trans.* **2021**, *50*, 9768−9774. (c) Zhao, X.-H.; Shao, D.; Chen, J.-T.; Gan, D.-X.; Yang, J.; Zhang, Y.-Z. A trinuclear $\{Fe^{III}_2Fe^{II}\}$ complex involving both spin and non-spin transitions exhibits three-step and wide thermal hysteresis. *Sci. China Chem.* **2022**, *65*, 532−538. (d) Liu, S.; Deng, Y.-F.; Chen, Z.-Y.; Meng, L.; Chang, X.-Y.; Zheng, Z.-P.; Zhang, Y.-Z. Secondary Metal Coordination Using a Tetranuclear Complex as Ligand Leading to Hexanuclear Complexes with Enhanced Thermal Barriers for Electron Transfer. *CCS Chem.* **2021**, *3*, 2530−2538. (e) Meng, L.-Y.; Deng, Y.-F.; Liu, S.; Zheng, Z.-P.; Zhang, Y.-Z. A smart post-synthetic route towards $[Fe_2Co_2]$ molecular capsules with electron transfer and bidirectional switching behaviors. *Sci. China Chem.* **2021**, *64*, 1340−1348.
(15) Deng, Y.-F.; Wang, Y.-N.; Zhao, X.-H.; Zhang, Y.-Z. Desolvation−Solvation-Induced Reversible On−Off Switching of Two Memory Channels in a Cobalt(II) Coordination Polymer: Overlay of Spin Crossover and Structural Phase Transition. *CCS Chem.* **2021**, *3*, 3277−3288.
(16) Ni, Z.-P.; Liu, J.-L.; Hoque, M. N.; Liu, W.; Li, J.-Y.; Chen, Y.-C.; Tong, M.-L. Recent Advances in Guest Effects on Spin-Crossover Behavior in Hofmann-Type Metal-Organic Frameworks. *Coord. Chem. Rev.* **2017**, *335*, 28−43.
(17) (a) Sciortino, N. F.; Scherl-Gruenwald, K. R.; Chastanet, G.; Halder, G. J.; Chapman, K. W.; Letard, J. F.; Kepert, C. J. Hysteretic Three-Step Spin Crossover in a Thermo-and Photochromic 3D Pillared Hofmann-type Metal-Organic Framework. *Angew. Chem., Int. Ed.* **2012**, *51*, 10154−10158. (b) Liu, W.; Peng, Y.-Y.; Wu, S.-G.; Chen, Y.-C.; Hoque, M. N.; Ni, Z.-P.; Chen, X.-M.; Tong, M.-L. Guest-Switchable Multi-Step Spin Transitions in an Amine-Functionalized Metal-Organic Framework. *Angew. Chem., Int. Ed.* **2017**, *56*, 14982−14986. (c) Clements, J. E.; Price, J. R.; Neville, S. M.; Kepert, C. J. Hysteretic Four-Step Spin Crossover within a Three-Dimensional Porous Hofmann-like Material. *Angew. Chem., Int. Ed.* **2016**, *55*, 15105−15109.
(18) Gütlich, P.; Garcia, Y.; Goodwin, H. A. Spin crossover phenomena in Fe(II) complexes. *Chem. Soc. Rev.* **2000**, *29*, 419−427.
(19) (a) Chen, Y.-C.; Meng, Y.; Dong, Y.-J.; Song, X.-W.; Huang, G.-Z.; Zhang, C.-L.; Ni, Z.-P.; Navarik, J.; Malina, O.; Zboril, R.; Tong, M.-L. Light-and temperature-assisted spin state annealing: accessing the hidden multistability. *Chem. Sci.* **2020**, *11*, 3281−3289. (b) Valverde-Muñoz, F. J.; Muñoz, M. C.; Ferrer, S.; BartualMurgui, C.; Real, J. A. Switchable Spin-Crossover Hofmann-Type 3D Coordination Polymers Based on Tri- and Tetratopic Ligands. *Inorg. Chem.* **2018**, *57*, 12195−12205. (c) Wang, L.-F.; Zhuang, W.-M.; Huang, G.-Z.; Chen, Y.-C.; Qiu, J.-Z.; Ni, Z.-P.; Tong, M.-L. Spin-Crossover Modulation via Single-Crystal to Single-Crystal Photochemical [2 + 2] Reaction in Hofmann-type Frameworks. *Chem. Sci.* **2019**, *10*, 7496−7502. (d) Dragulescu-Andrasi, A.; Hietsoi, O.; Üngör, Ö.; Dunk, P. W.; Stubbs, V.; Arroyave, A.; Kovnir, K.; Shatruk, M. Dicyanometalates as Building Blocks for Multinuclear Iron(II) Spin-Crossover Complexes. *Inorg. Chem.* **2019**, *58*, 11920−11926.
(20) Benchohra, A.; Li, Y.; Chamoreau, L. M.; Baptiste, B.; Elkaim, E.; Guillou, N.; Kreher, D.; Lescouëzec, R. The Atypical Hysteresis of $[Fe(C_6F_5Tp)_2]$: Overlay of Spin-Crossovers and Symmetry-Breaking Phase Transition. *Angew. Chem., Int. Ed.* **2021**, *60*, 8803−8807.
(21) Rosario-Amorin, D.; Dechambenoit, P.; Bentaleb, A.; Rouzieres, M.; Mathonière, C.; Clérac, R. Multistability at Room Temperature in a Bent-Shaped Spin-Crossover Complex Decorated with Long Alkyl Chains. *J. Am. Chem. Soc.* **2018**, *140*, 98−101.
(22) (a) Shatruk, M.; Phan, H.; Chrisostomo, B. A.; Suleimenova, A. Symmetry-Breaking Structural Phase Transitions in Spin Crossover Complexes. *Coord. Chem. Rev.* **2015**, *289*−*290*, 62−73. (b) Xue, S.; Guo, Y.; Garcia, Y. Spin crossover crystalline materials engineered via single-crystal-to-single-crystal transformations. *CrystEngComm.* **2021**, *23*, 7899−915.
(23) (a) Qiu, Y.-R.; Cui, L.; Cai, P.-Y.; Yu, F.; Kurmoo, M.; Leong, C. F.; D'Alessandro, D. M.; Zuo, J.-L. Enhanced dielectricity coupled to spin-crossover in a one-dimensional polymer iron(ii) incorporating tetrathiafulvalene. *Chem. Sci.* **2020**, *11*, 6229−6235. (b) Wu, S.-G.; Hoque, M. N.; Zheng, J.-Y.; Huang, G.-Z.; Ha Anh, N. V.; Ungur, L.; Zhang, W.-X.; Ni, Z.-P.; Tong, M.-L. Multiresponsive Spin Crossover Driven by Rotation of Tetraphenylborate Anion in an Iron(III) Complex. *CCS Chem.* **2021**, *3*, 453−459.

https://doi.org/10.1021/acs.inorgchem.2c00192
Inorg. Chem. 2022, 61, 5855−5860